

Topological transitions from multipartite entanglement with tensor networks: a procedure for sharper and faster characterization

Román Orús,¹ Tzu-Chieh Wei,² Oliver Buerschaper,^{3,4} and Artur García-Saenz²

¹*Institute of Physics, Johannes Gutenberg University, 55099 Mainz, Germany*

²*C. N. Yang Institute for Theoretical Physics, State University of New York at Stony Brook, NY 11794-3840, USA*

³*Perimeter Institute for Theoretical Physics, 31 Caroline Street North, Waterloo, Ontario, Canada, N2L 2Y5*

⁴*Dahlem Center for Complex Quantum Systems,
Freie Universität Berlin, 14195 Berlin, Germany*

Topological order in a 2d quantum matter can be determined by the topological contribution to the entanglement Rényi entropies. However, when close to a quantum phase transition, its calculation becomes cumbersome. Here we show how topological phase transitions in 2d systems can be much better assessed by multipartite entanglement, as measured by the topological geometric entanglement of blocks. Specifically, we present an efficient tensor network algorithm based on Projected Entangled Pair States to compute this quantity for a torus partitioned into cylinders, and then use this method to find sharp evidence of topological phase transitions in 2d systems with a string-tension perturbation. When compared to tensor network methods for Rényi entropies, our approach produces almost perfect accuracies close to criticality and, on top, is orders of magnitude faster. The method can be adapted to deal with any topological state of the system, including minimally entangled ground states. It also allows to extract the critical exponent of the correlation length, and shows that there is no continuous entanglement-loss along renormalization group flows in topological phases.

PACS numbers: 75.10.Jm, 05.30.Pr, 03.67.Mn

Topological order [1] is a striking property of quantum matter beyond the Landau paradigm and is characterized by an underlying pattern of long-range entanglement. The existence of such a pattern can be detected, quantitatively, by the so-called topological entanglement entropy S_γ [2]. Other entanglement properties are sensitive to topological order as well [3]. Moreover, under the effect of a local perturbation it is also well-known that topological order is generally robust [4, 5] and can sustain a finite perturbation. Intuitively, large closed strings and string-nets become energetically expensive in a topological phase as a string-tension is increased, thus ultimately favoring a transition towards a topologically-trivial phase. A drawback of using entanglement to detect such topological transitions, however, is that it is very difficult to produce sharp numerical evidence. The reason for this is that commonly used methods, such as the calculation of the topological contribution in Rényi entropies [6], suffer from a significant drop in accuracy when close to a quantum critical point [7], see Fig. 1. Here we show how multipartite entanglement, in combination with tensor networks, improves accuracies to an almost perfect level and, on top, is computed orders of magnitude faster than any Rényi entropy.

More specifically, here we use a *novel and efficient tensor network method to evaluate the topological contribution to the geometric entanglement (GE) of blocks, which we call E_γ , for a torus partitioned into cylinders*. When close to a quantum phase transition, we find that this approach completely outperforms in accuracy and efficiency calculations of Rényi entropies on infinite cylinders with tensor networks [30]. Without describing the technical

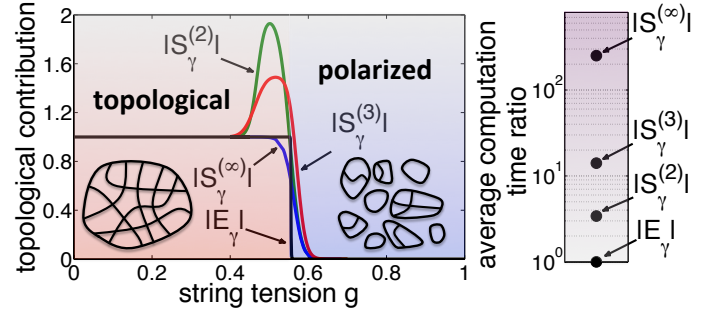


FIG. 1: (color online) Left: phase transition for a topological 2d model with string tension. The black line corresponds to $|E_\gamma|$ as computed in Fig. 4(a) for $n_b \rightarrow \infty$ using GE (to be explained later). The rest of the lines correspond to the best achievable calculation by the authors of the topological term $|S_\gamma^{(n)}|$ of the n th Rényi entropies $S^{(n)} = (1-n)^{-1} \log(\text{tr}(\rho^n))$ of half an infinite cylinder for $n = 2, 3$ and $n = \infty$ (i.e. the single-copy entanglement [10]), using the methods explained in the supplementary material. Compare also to similar calculations with tensor networks in, e.g., Ref. [7]. Typical sizes of string-nets populating the ground state for each phase are also represented. Right: average computation time ratio with respect to $|E_\gamma|$, for the different topological contributions.

details, the main result is summarized in Fig. 1. We apply a string tension g (which corresponds to a magnetic field in the Hamiltonian [8, 9]) to certain toric code ground states, and compute the topological contribution of the GE of these “strained” toric code states. Unlike the topological Rényi entropies, the computed E_γ stays close to -1 throughout the entire topological phase and, as the

string tension increases, it sharply drops down to zero at $g^* \approx 0.56$ and remains there in the trivial phase. From a mapping to a classical 2D Ising model [8] we obtain analytically a transition at $g^* = \sqrt{1 + \sqrt{2}} - 1 \approx 0.5537$, in agreement with the above. E_γ is thus an excellent tool to pinpoint topological phase transitions.

Our method uses Projected Entangled Pair States (PEPS) [12]. If the PEPS is topological [13], then a robust E_γ is extracted via finite-size scaling for large toruses. For non-trivial partitions we find E_γ to depend on the particular superposition of ground states on the torus, in agreement with the behavior of Rényi entropies and entanglement entropy [14]. Our calculations focus mainly on PEPS with a translation invariant representation. This has two main advantages: first, it simplifies the calculations, and second, it corresponds to the type of unique ground state of a topological system that can be found on an infinite plane using, e.g., the iPEPS method [15]. Even if such states have a weaker topological contribution on a torus than minimally entangled states (MES), they are much simpler to deal with, and already produce non-trivial topological contributions. In any case, we shall see that our method can be easily extended to PEPS representations that are not invariant under translations, thus including MES if necessary. Importantly, with this method we also have access to other properties. For instance, in the supplementary material we show how to extract the critical exponent ν , and how to see that there is no continuous entanglement-loss along renormalization group flows in topological phases [16] together with a fidelity analysis [17].

GE and topological GE — The geometric entanglement of blocks [18, 19] has recently proven useful to assess topological order [20, 21]. This multipartite measure has been extensively used in quantum phase transitions [22], and can be measured experimentally, e.g., in NMR [23] and potentially in optical lattice experiments [24]. In contrast to all other entanglement approaches for topological matter, the GE takes into account the multipartite structure of entanglement in quantum many-body states. It amounts to computing the closest product state $|\Phi\rangle$ to a given quantum state $|\Psi\rangle$ in the Hilbert space, where the product state has a separable structure of n_b blocks, i.e., $|\Phi\rangle = \prod_{i=1}^{n_b} |\phi^{[i]}\rangle$. It thus quantifies the merit of a possible mean-field description of the quantum state. Conveniently, the GE is defined as $E_G \equiv -\log |\langle \Phi | \Psi \rangle|^2$.

One of the latest findings has been that, for renormalization group (RG) fixed points such as the toric code and other topological exactly-solvable models, the GE of blocks obeys $E_G = E_0 - E_\gamma$, with E_γ a topological contribution (the topological GE) and E_0 some non-universal term [20]. It was observed that $E_\gamma = S_\gamma$ for the considered models. This constant contribution was shown to be directly connected to the size of the gauge group, which in turn governs topological order in

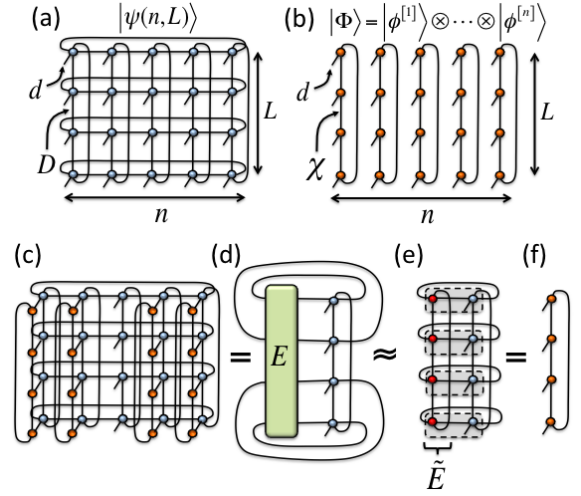


FIG. 2: (color online) (a) PEPS $|\Psi(n, L)\rangle$ wrapped around a torus. (b) Product state $|\Phi\rangle$ of MPSs with pbc (cylinders with $l = 1$). (c) Contraction to compute the optimal state for a given cylinder. (d) Exact result of the contraction in terms of the environment tensor E . (e) Approximation of E by an effective environment \tilde{E} described by an MPO. (f) Resulting optimal MPS for the cylinder in an iteration step (see main text).

the system. As for E_0 it was found that $E_0 \propto n_b L$, with n_b the number of blocks with a contractible boundary of size L . Moreover, under perturbations it was argued that $E_G = E_0 - E_\gamma + O(L^{-\nu'})$ for $L \gg 1$, where again $E_0 \propto n_b L$, ν' is some exponent, and E_γ is the (robust) topological term. Recently, the topological GE has also been used to identify minimally-entangled ground states, both for abelian and non-abelian models [21].

Computing E_G and E_γ from a PEPS — Our approach to computing the GE of non-contractible blocks E_G for large block sizes and its topological contribution E_γ uses 2d PEPS and 1d Matrix Product States (MPS). Both PEPS and MPS have been widely discussed in the literature (see, e.g., Ref.[25]). It is worth mentioning that PEPS can describe 2d topological phases naturally, both chiral [26] and non-chiral (or doubled) [13]. For simplicity, here we focus on non-chiral topological order, but a generalization of our method to chiral models is also possible.

As a starting point we assume that a PEPS $|\Psi\rangle$ with (potentially) topological order is given on a torus of $n \times L$ sites, see Fig.2(a). We call such a state $|\Psi(n, L)\rangle$. This PEPS could be the result of an analytical derivation, or have been computed numerically from a Hamiltonian using, e.g., the iPEPS algorithm [15] and wrapping later its tensors around a finite torus.

The goal now is to extract E_G and E_γ from such a PEPS. With this in mind, we partition the torus into n_b cylinders of equal width $l = n/n_b$. Thus each cylinder contains $l \times L$ sites, see, e.g., Fig.2(b). This choice of

partition will have a double benefit. First, it will simplify the tensor contractions in the method. Second, it will be sensitive to different ground states on the torus, and hence to MES.

We focus on the case $l = 1$, so that $n_b = n$. In this case, one needs to find the closest product state $|\Phi\rangle = \otimes_{i=1}^{n_b} |\phi^{[i]}\rangle$ of cylinders of one-site width to $|\Psi(n, L)\rangle$, with $|\phi^{[i]}\rangle$ the state for cylinder i . To do such a calculation efficiently, we further approximate $|\phi^{[i]}\rangle$ for each cylinder by an MPS of L sites with periodic boundary conditions (pbc) and bond dimension χ , see Fig.2(b) [31]. Thus, the original problem is reduced to finding the product state of MPSs with pbc that maximizes the overlap with a given PEPS on a torus, which is a well-posed tensor network problem.

In what follows we describe an optimization procedure, well-suited for gapped topological phases, to solve this problem. The method assumes a translation invariant PEPS, but it can also be generalized to PEPS without translation symmetry (such as MESs).

1.- Assume translation invariance so that cylinders are repeated periodically. While not necessary for a finite system, this assumption simplifies the calculations and also produces good results for translation invariant PEPS. Here a 2-cylinder unit-cell is already sufficient, but bigger unit cells can also be considered.

2.- Fix all tensors in the MPSs to some initial (e.g., random) values except for one cylinder, and optimize variationally the MPS tensors for that cylinder. The result of this optimization is given by the diagram in Fig.2(c,d). Notice, though, that for a 2d lattice the environment tensor E cannot be computed both exactly and efficiently, and therefore needs to be approximated.

3.- Compute an effective environment \tilde{E} approximating the exact environment E , using some method to approximate contractions of 2d tensor networks. In our case we assume further translation invariance within each cylinder, and use the iTEBD method for non-unitary evolutions [27, 28], without explicitly implementing the boundary conditions imposed by the torus geometry, and adapted to deal with Matrix Product Operators (MPO). The specifics are explained in the supplementary material. As a result of this approach, an infinite MPO of bond dimension χ' is produced which is then cut at length L and wrapped around a circle with pbc. Such an approximation is particularly accurate for large L and gapped phases, which is precisely the regime of interest to extract E_γ . This finite MPO with pbc describes the effective environment \tilde{E} , see Fig.2(e).

4.- Approximate the optimal MPS for the cylinder as in Fig.2(f).

5.- Substitute this MPS in all the equivalent cylinders by translation invariance.

6.- Repeat the procedure for the next cylinder in the unit cell.

7.- Iterate until convergence.

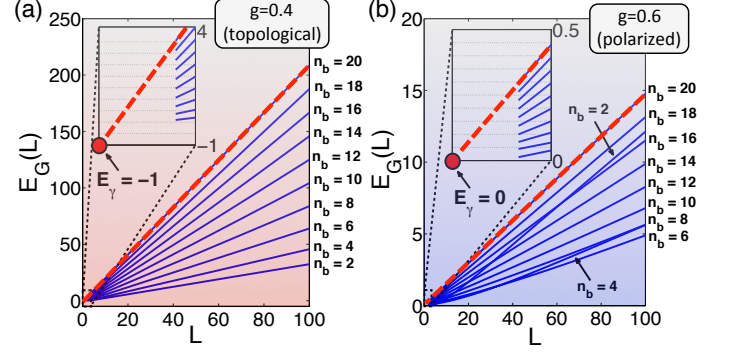


FIG. 3: (color online) $E_G(n, L)$ for the toric code with string tension on the square lattice (similar results are also obtained for the honeycomb lattice). (a) Case $g = 0.4$. The extrapolation of the linear fit (red dashed line) for, e.g., $n = 20$ hits $L = 0$ around ~ -1 (red dot), as expected in the topological phase. (b) Case $g = 0.6$. The same calculation yields ~ 0 , as expected in the polarized phase.

The optimal overlap is thus evaluated as

$$\Lambda_{\max}(n, L) \simeq \frac{|\langle \Phi | \Psi(n, L) \rangle|}{\sqrt{|\langle \Phi | \Phi \rangle| |\langle \Psi(n, L) | \Psi(n, L) \rangle|}}, \quad (1)$$

with $|\Phi\rangle = \otimes_{i=1}^{n_b} |\phi^{[i]}\rangle$, and $|\phi^{[i]}\rangle$ the optimal MPS for each cylinder. In this expression, the numerator can be approximated using, e.g., the procedure described in the first section of the supplementary material with a computational cost of $O(n_b \chi^3 \chi'^3 D^5 + L \chi'^3)$. The norm of $|\Phi\rangle$ is simply the product of the norms of the n_b MPS of size L with pbc, which can be evaluated exactly and efficiently in $O(L \chi'^5)$ steps (see, e.g., [25]). The norm of the $n \times L$ PEPS $|\Psi(n, L)\rangle$ can be approximated as in the first section of the supplementary material with a computational cost of $O(n(\chi''^2 D^9 + \chi''^3 D^6) + L \chi''^3)$, with χ'' the bond dimension of the needed MPO. Finally, the GE is given by $E_G(n, L) \equiv -\log_2 \Lambda_{\max}^2(n, L)$.

For an $n \times L$ PEPS on a torus it is thus possible to approximate $E_G(n, L)$ as above. To get the topological contribution, the next step is to perform *finite-size scaling* with respect to n and L . In particular, we have $E_G(n \gg 1, L \gg 1) \sim \alpha n L - E_\gamma(n, L)$, where $E_\gamma(n, L)$ includes both the topological component E_γ as well as finite-size corrections. We can then fix n and compute $E_G(n, L)$ for increasing L . Doing a linear fit for large L allows us to extract an approximation to the topological GE by extrapolating the fit down to $L = 0$. The larger n is, the more accurate the approximation is. Thus, the value of the topological correction is finally estimated as $E_\gamma = \lim_{n, L \rightarrow \infty} E_\gamma(n, L)$.

Some remarks are in order. First, accuracy can always be improved by increasing the different bond dimensions, or by applying tensor network methods that explicitly take into account pbc rather than iTEBD, or by using larger unit cells (and even breaking completely translation invariance along any direction) in the product state

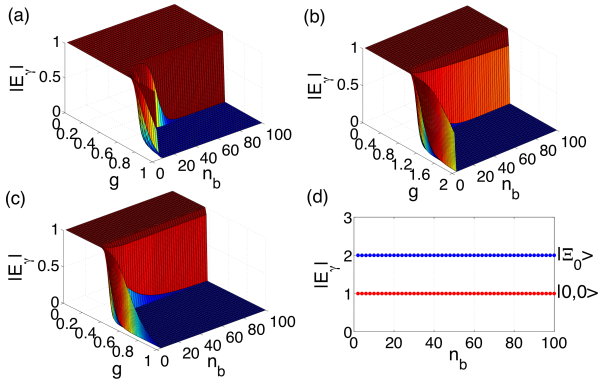


FIG. 4: (color online) absolute value of E_γ extrapolated from the scaling with L as in Fig.(3), as a function of the string tension g (for a-c) and the number of blocks n_b (for a-d). Plots are for the perturbed (a) $|0,0\rangle$ state on the square lattice, (b) $|0,0\rangle$ state on the honeycomb lattice, and (c) $|+,+\rangle$ state on the honeycomb lattice. Notice that (b) and (c), though being ground states on the same lattice, have different transition points. This is because the string tension g was applied in different bases, hence corresponds to different physical perturbations. However, we have also checked that, when the *same* perturbation is applied to different ground states on the same lattice, the topological phase transition takes place at the same critical point, showing that the transitions in E_γ do *not* depend on the specific choice of ground state. Figure (d) corresponds to the unperturbed toric code on a square lattice for two different ground states: an MES $|\Xi_0\rangle$, and a non-MES $|0,0\rangle$.

$|\Phi\rangle$. Second, cylinders of larger width $l > 1$ can be considered by using a PEPS for an l -leg ladder with pbc to approximate the state $|\phi^{[i]}\rangle$ within each cylinder, or perhaps even an MPS with pbc and physical dimension d^l (with d the physical dimension of a single site). An example of such a calculation is shown in the supplementary material. Third, MESs can also be studied introducing minor changes in the method. For this, notice that the PEPS representation of an MES is translation invariant except for, e.g., one cylinder where a Wilson loop operator acted. Thus, one chooses $|\Phi\rangle$ as a translation invariant product state of MPSs, except for the Wilson loop cylinder, where a different MPS is chosen. The rest of the method just follows. Fourth, the method relies on single-layer contractions of a $2d$ tensor network, which are computed both more efficiently and more accurately than the double-layer contractions in Rényi entropy calculations. This is model-independent, and explains the overall computational gain from Fig.1. A more detailed justification is provided in the supplementary material.

Topological phase transitions from E_γ — Using the above method we computed E_G and E_γ for the toric code model [4] with string tension on the square and honeycomb lattices. Details about the PEPS for these models as well as about the blocking schemes are given in the supplementary material. The string tension g

drives the systems towards a phase transition between topological and polarized phases. Using the notation from Ref.[20], we considered perturbations to two non-equivalent ground states $|0,0\rangle$ and $|+,+\rangle$ for the honeycomb lattice, whereas for the square lattice we considered perturbations to the $|0,0\rangle$ state. In the topological phase, these states are the unique ground states of the system on an infinite plane, but on a torus they correspond to a superposition of MESs with topological entropy $S_\gamma = -1$ for a non-contractible bipartition [14].

Our calculations were done for toruses up to $n = 100$ and $L = 100$. Larger sizes could have easily been considered if necessary. In Fig.3 we show an example of the scalings with L for different values of n up to $n = 20$ for two different string tensions $g = 0.4, 0.6$ on the square lattice. The linear fit is computed from the last half of L values, which produces robust results. In the plots, the extrapolation of the fit to $L = 0$ hits the vertical axis around -1 if g is small, corresponding to the topological phase, and around 0 for large g , corresponding to the polarized phase. From the fits we can extract E_γ as a function of $n = n_b$ and g , as shown in Fig.4(a-c) for the three states considered. Remarkably, these plots show very sharp indications of topological phase transitions for all these models for large n_b . With this approach we also extracted E_γ for one of the MES of the square toric code on a torus without perturbation. Specifically, we considered the state $|\Xi_0\rangle \equiv 2^{-1/2}(|0,0\rangle + |1,0\rangle)$ (in the notation of Ref.[20]) which has $S_\gamma = -2$ for a non-trivial torus bipartition [14]. Remarkably, we also find $E_\gamma = -2$ for this state, see Fig.4(d).

Conclusions — We obtained sharp evidence of topological quantum phase transitions for 2d systems, by calculating E_γ using a new and efficient tensor network method for non-trivial partitions on a torus. Our method completely outperforms similar tensor network calculations of Rényi entropies for infinite cylinders, by being orders of magnitude more accurate and efficient close to criticality [7]. This approach can also be applied to different ground states, including MES, and allows to extract other non-trivial information about the system (e.g., correlation length critical exponent, and lack of continuous entanglement loss along RG flows in topological phases). Our work motivates further research along several directions. For instance, it would be possible to use these tools to study chiral topological order [29], topological critical exponents, and MES. Beyond tensor network methods, it would be interesting to study how to compute E_γ using Quantum Monte Carlo, and compare the accuracy and efficiency to that of 2-Rényi entropy calculations.

Discussions with B. Bauer, F. Pollmann, A. Sanpera and G. Vidal are acknowledged. T.-C.W. and A.G.-S. acknowledge the support by the National Science Foundation under Grants No. PHY 1314748 and No. PHY 1333903.

-
- [1] X.-G. Wen, *Quantum Field Theory of Many-Body Systems* (Oxford University Press, USA, 2004).
- [2] A. Kitaev and J. Preskill, Phys. Rev. Lett. **96**, 110404 (2006); M. Levin, X.-G. Wen, *ibid* **96**, 110405 (2006).
- [3] S. Iblisdir *et al.*, Phys. Rev. B **79**, 134303 (2009); Y. Arthur Lee, G. Vidal, Phys. Rev. A **88**, 042318 (2013); C. Castelnovo, Phys. Rev. A **88**, 042319 (2013).
- [4] A. Y. Kitaev, Annals of Physics 303, 2-30 (2003).
- [5] A. Hamma D. A. Lidar, Phys. Rev. Lett. **100**, 030502 (2008); S. Trebst *et al.*, Phys. Rev. Lett. **98**, 070602 (2007); I. S. Tupitsyn *et al.*, Phys. Rev. B **82**, 085114 (2010); J. Vidal, S. Dusuel, K. P. Schmidt, Phys. Rev. B **79**, 033109 (2009); J. Vidal *et al.*, Phys. Rev. B **80**, 081104(R) (2009); J. Yu, S.-P. Kou, X.-G. Wen, Europhys. Lett. **84**, 17004 (2008); X.-G. Wen, Phys. Rev. Lett. **90**, 016803 (2003); S. Dusuel *et al.*, Phys. Rev. Lett. **106**, 107203 (2011); L. Tagliacozzo, G. Vidal, Phys. Rev. B **83**, 115127 (2011); M. D. Schulz *et al.*, New J. Phys. **14** 025005 (2012); H. He, H. Moradi, X.-G. Wen, arXiv:1401.5557; S. Bravyi, M. Hastings, S. Michalakakis, J. Math. Phys. **51**, 093512 (2010); S. Michalakakis, M. Zwolak, Commun. Math. Phys. **322**, pp. 277302 (2013).
- [6] S. T. Flammia *et al.*, Phys. Rev. Lett. **103**, 261601 (2009).
- [7] S. V. Isakov *et al.*, Nature Physics **7**, 772 (2011); X. Chen *et al.*, Phys. Rev. B **82**, 165119 (2010); S. Morampudi, C. von Keyserlingk, F. Pollmann, arXiv:1403.0768; J.-M. Stéphan, G. Misguich, V. Pasquier, J. Stat. Mech. P02003 (2012).
- [8] C. Castelnovo and C. Chamon, Phys. Rev. B **77**, 054433 (2008).
- [9] S. Trebst, P. Werner, M. Troyer, K. Shtengel, C. Nayak, Phys. Rev. Lett. **98**, 070602 (2007). N. Schuch, D. Poilblanc, J. I. Cirac, and David Pérez-García, Phys. Rev. Lett. **111**, 090501 (2013).
- [10] J. Eisert, M. Cramer, Phys. Rev. A **72**, 042112 (2005); R. Orús *et al.*, Phys. Rev. A **73**, 060303(R) (2006).
- [11] J. I. Cirac *et al.*, Phys. Rev. B **83**, 245134 (2011).
- [12] F. Verstraete, J. I. Cirac, arXiv:cond-mat/0407066.
- [13] F. Verstraete and J. I. Cirac, Phys. Rev. A **70**, 060302(R) (2004); F. Verstraete, M. M. Wolf, D. Perez-García, and J. I. Cirac, Phys. Rev. Lett. **96**, 220601 (2006); O. Buereschaper, M. Aguado, G. Vidal, Phys. Rev. B **79**, 085119 (2009); Z.-Cheng Gu *et al.*, Phys. Rev. B **79**, 085118 (2009); R. Orús, Annals of Physics **349**, 117158 (2014).
- [14] S. Dong *et al.*, J. High Energy Phys. **05** 016 (2008); Y. Zhang *et al.*, Phys. Rev. B **85**, 235151 (2012).
- [15] J. Jordan *et al.*, Phys. Rev. Lett. **101**, 250602 (2008); R. Orús, G. Vidal, Phys. Rev. B **80**, 094403 (2009).
- [16] B. Swingle, arXiv:1307.8117; S. Santra *et al.*, arXiv:1310.6490; J.I. Latorre *et al.*, Phys. Rev. A **71** 034301 (2005); R. Orús, Phys. Rev. A **71**, 052327 (2005), erratum-*ibid* **73**, 019904 (2006); A. B. Zamolodchikov, JETP Lett. **43** 730 (1986); I. R. Klebanov, S. S. Pufu, B. R. Safdi, arXiv:1105.4598.
- [17] P. Zanardi and N. Paunković, Phys. Rev. E **74**, 031123 (2006); H.-Q. Zhou, J.P. Barjaktarevic, cond-mat/0701608; H.-Q. Zhou, J.-H. Zhao, B. Li, arXiv:0704.2940; H.-Q. Zhou, arXiv:0704.2945; H.-Q. Zhou, R. Orús, G. Vidal, Phys. Rev. Lett. **100**, 080601 (2008).
- [18] T.-C. Wei and P. M. Goldbart, Phys. Rev. A **68**, 042307 (2003).
- [19] A. Botero and B. Reznik, arXiv:0708.3391; R. Orús, Phys. Rev. Lett. **100**, 130502 (2008).
- [20] R. Orús *et al.*, New J. Phys. **16** 013015 (2014).
- [21] O. Buereschaper, A. García-Saenz, R. Orús, T.-C. Wei, J. Stat. Mech. 2014, P11009.
- [22] R. Orús, Phys. Rev. A **78**, 062332 (2008); T.-C. Wei, *ibid* **81**, 062313 (2010); T.-C. Wei *et al.*, Phys. Rev. A **71**, 060305(R) (2005); R. Orús, S. Dusuel and J. Vidal, Phys. Rev. Lett. **101**, 025701 (2008).
- [23] J. Zhang, T.-C. Wei and R. Laflamme, Phys. Rev. Lett. **107**, 010501 (2011).
- [24] A. J. Daley, H. Pichler, J. Schachenmayer and P. Zoller, Phys. Rev. Lett. **109**, 020505 (2012).
- [25] R. Orús, Annals of Physics 349 (2014) 117-158; R. Orús, arXiv:1407.6552 (to appear in EPJB); J. I. Cirac, F. Verstraete, J. Phys. A: Math. Theor. **42**, 504004 (2009); F. Verstraete, J. I. Cirac, V. Murg, Adv. Phys. **57**, 143 (2008); R. Augusiak, F. M. Cucchietti, M. Lewenstein, in *Modern Theories of Many-Particle Systems in Condensed Matter Physics*, Lect. Not. Phys. **843**, 245-294 (2012); U. Schollwöck, Rev. Mod. Phys. **77**, 259 (2005); U. Schollwöck, Ann. Phys. **326**, 96 (2011).
- [26] J. Dubail, N. Read, arXiv:1307.7726; T.B. Wahl *et al.*, Phys. Rev. Lett. **111**, 236805 (2013).
- [27] G. Vidal, Phys. Rev. Lett. **98**, 070201 (2007).
- [28] R. Orús, G. Vidal, Phys. Rev. B **78**, 155117 (2008).
- [29] M. P. Zaletel, R. S. K. Mong, F. Pollmann, Phys. Rev. Lett. **110**, 236801 (2013).
- [30] See, e.g., Ref.[11], as well as the supplementary material for the specific algorithms implemented to obtain the data in Fig.1.
- [31] This is indeed justified, as we show in the supplementary material.

SUPPLEMENTARY MATERIAL

In this supplementary material we provide details on the following:

1. Tensors for the toric code model with string tension on different lattices.
2. Calculation of the effective environment using iTEBD and MPOs.
3. Blocking of spins on the square and honeycomb lattices.
4. Extracting E_γ using cylinders of width $l = 2$ on the square lattice.
5. Alternative optimization strategies and finite-size effects in E_G .
6. Fidelity diagram and no entanglement loss along RG flows in topological phases.
7. Extracting the critical exponent ν from the finite-size scaling of E_γ .
8. Efficient methods to compute the n th-Rényi entropy and its topological contribution, for finite and infinite n , for a 2d PEPS on an infinite cylinder.
9. Numerical truncation errors in E_G and Rényi entropies.

1. Tensors for the toric code with a string tension

As examples of perturbed topological models, in this paper we have considered Kitaev's toric code model [3] with a string tension on square and honeycomb lattices. It is well known that the ground states for these systems on an infinite plane can always be specified by a PEPS. Here we adopt the convention that tensor bond indices are subscripts, starting from the leftmost index in the lattice and following a clockwise rotation order, and physical indices are superscripts. Details on how to derive the PEPS tensors for the toric code can be found on, e.g., Ref.[4]. According to this convention, and following the notation of Ref.[5] for the toric code ground states, the three PEPS that we consider here are:

(i) *Perturbed $|0,0\rangle$ ground state on the square lattice.* This is described by 2 PEPS tensors A and B with bond dimension $D = 2$. The non-zero coefficients $A_{\alpha\beta\gamma\delta}^i$ (where i and $\alpha \dots \gamma$ are the physical and bond indices respectively) are given by

$$\begin{aligned} A_{1,1,1,1}^1 &= 1 + g & A_{2,2,1,1}^2 &= 1 \\ A_{2,2,2,2}^1 &= 1 + g & A_{1,1,2,2}^2 &= 1 \end{aligned} \quad (2)$$

with g a string tension, and B being a rotation of $\pi/2$ of A on the lattice.

(ii) *Perturbed $|0,0\rangle$ ground state on the honeycomb lattice.* This is described by two tensors T and Δ with non-zero coefficients

$$\begin{aligned} T_{1,1}^1 &= 1 + g & T_{1,2}^2 &= 1 \\ T_{2,2}^1 &= 1 + g & T_{2,1}^2 &= 1 \end{aligned} \quad (3)$$

and

$$\Delta_{1,1,1} = \Delta_{2,2,2} = 1, \quad (4)$$

see Fig.5. A more convenient description for the numerical calculations is given in terms of tensors A and B computed from T and Δ as shown in Fig.5. In this construction the PEPS bond dimension is $D = 2$, whereas the physical dimensions are 2 for A and 4 for B .

(iii) *Perturbed $|+,+\rangle$ ground state on the honeycomb lattice.* This is described by tensors T , Δ and $\tilde{\Delta}$ with non-zero coefficients

$$\begin{aligned} T_{1,1}^+ &= 1 + g & T_{2,2}^- &= 1 \\ T_{4,4}^+ &= 1 + g & T_{3,3}^- &= 1 \end{aligned} \quad (5)$$

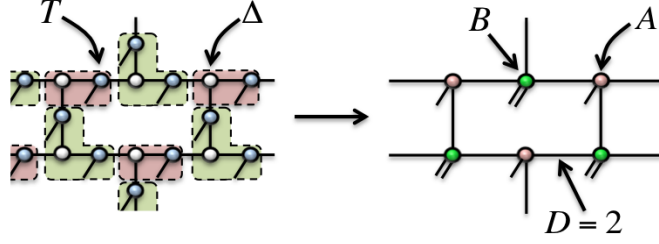


FIG. 5: (color online) tensors for the PEPS $|0,0\rangle$ perturbed ground state on the honeycomb lattice. The lattice is represented as a brickwall.

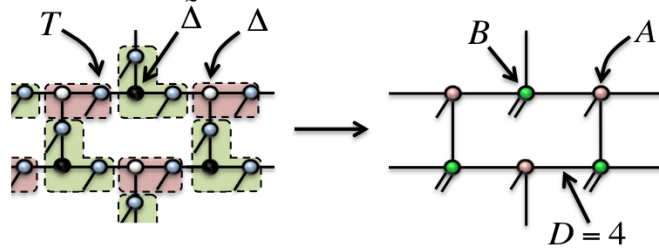


FIG. 6: (color online) tensors for the PEPS $|+,+\rangle$ perturbed ground state on the honeycomb lattice. The lattice is represented as a brickwall.

$$\begin{aligned} \Delta_{1,1,1} &= \Delta_{3,3,1} = \Delta_{2,1,3} = \Delta_{1,2,2} = 1 \\ \Delta_{4,3,3} &= \Delta_{3,4,2} = \Delta_{2,2,4} = \Delta_{4,4,4} = 1 \end{aligned} \quad (6)$$

$$\begin{aligned} \tilde{\Delta}_{1,1,1} &= \tilde{\Delta}_{3,3,1} = \tilde{\Delta}_{1,2,3} = \tilde{\Delta}_{2,1,2} = 1 \\ \tilde{\Delta}_{3,4,3} &= \tilde{\Delta}_{4,3,2} = \tilde{\Delta}_{2,2,4} = \tilde{\Delta}_{4,4,4} = 1, \end{aligned} \quad (7)$$

see Fig.6. One can rewrite again the tensor network in terms of two tensors A and B as shown in Fig.6. This time, the PEPS bond dimension is $D = 4$, and the physical dimensions are again 2 for A and 4 for B .

Remarks

The above perturbations on the $|0,0\rangle$ and $|+,+\rangle$ states on the honeycomb lattice correspond, in fact, to different physical perturbations: one adds weight to strings of 1's or + 's respectively. It is, however, easy to apply the same perturbation to both ground states. For instance, in the $\{|1\rangle, |2\rangle\}$ basis for every spin, the perturbed $|0,0\rangle$ state can be written as $Q^{\otimes N}|0,0\rangle$, with N the number of spins and $Q = (1+g)|1\rangle\langle 1| + |2\rangle\langle 2|$. The perturbed $|+,+\rangle$ state after applying the *same* perturbation Q to every spin then reads $Q^{\otimes N}|+,+\rangle$, and the PEPS for such a state is easy to compute in the $\{|+\rangle, |-\rangle\}$ local basis (with $|\pm\rangle = (|1\rangle \pm |2\rangle)/\sqrt{2}$) and noticing that the perturbation operator can be written as $Q = (1+g/2)(|+\rangle\langle +| + |-\rangle\langle -|) + (g/2)(|+\rangle\langle -| + |-\rangle\langle +|)$

2. Computation of the effective environment \tilde{E} as an MPO using iTEBD

At several points in our numerical methods we use iTEBD to produce an MPO approximation of the multiplication of several transfer operators, e.g., when computing the exact environment E for E_G in step 3. To do so, we assume that we have translation invariance every, e.g., 2 lattice sites at least. This MPO is produced is as follows:

1.- *Contract* the tensors for two columns as in Fig.7(a). This is the product of two infinite MPOs. If both MPOs have bond dimension D , then the resulting MPO will have bond dimension D^2 .

2.- *Find the canonical form* of the resulting MPO, see Fig.7(b,c). This can be done using the algorithms from Ref.[1, 2], adapted to an MPS with two physical legs per site of dimension D each.

3.- *Truncate* the bond dimension of the MPO to its largest χ' Schmidt coefficients of a bipartition across each link, see Fig.7(d).

4.- *Absorb* the Schmidt coefficients into the tensors at each site, see Fig.7(e).

5.- *Iterate* until approximating the contraction of $n_b - 1$ infinite columns. At each iteration step we will have as input two infinite MPOs, one of bond dimension χ' and another one of bond dimension D . The output will always be a new infinite MPO of bond dimension χ' .

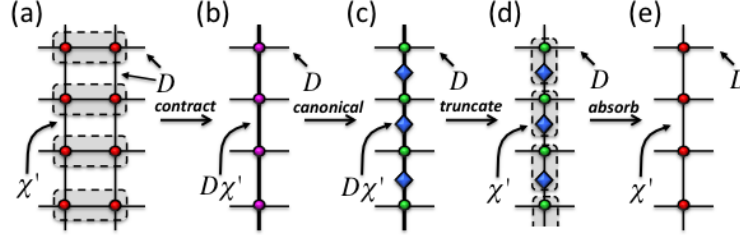


FIG. 7: (color online) iTEBD method for non-unitary MPOs, adapted from Ref.[2]. (a) Contraction of 2 MPOs of bond dimensions χ' and D . (b) Resulting MPO of bond dimension $D\chi'$. (c) Canonical form of the MPO in (b), in terms of MPO tensors (circles) and matrices of Schmidt coefficients (diamonds). (d) Truncated MPO of bond dimension χ' in canonical form. (e) Final MPO, where we have absorbed the Schmidt coefficients into the tensors at each site.

3. Choice of blocking

In Fig.8 we show our explicit choice of blocks for the square and honeycomb lattices, for the case of blocks of width $l = 1$. Larger widths can be considered easily following this scheme. In the lattices, spins are on the links.

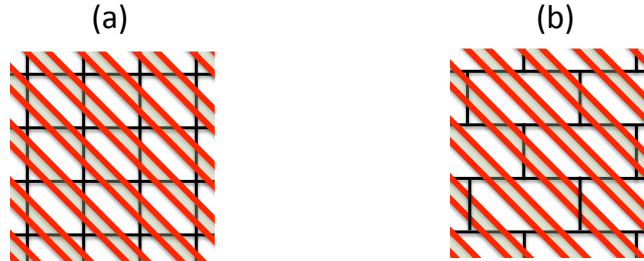


FIG. 8: (color online) Blocking of spins for (a) square lattice, and (b) honeycomb lattice. Spins are on the links.

4. Extracting E_γ using cylinders of width $l = 2$

As a proof of principle, we have done a calculation for cylinders with a width of more than one site, namely $l = 2$. For toruses up to 100×100 sites, this implies that n_b reaches up to 50 cylinders. In Fig.9 we see an example of such a calculation for the perturbed toric code ground state on the square lattice, and compare it to that of Fig.4(a). As expected, we see convergence with n_b twice as fast as compared to the case $l = 1$, showing the same estimation for the quantum critical point $g^* \approx 0.56$.

5. Alternative optimization strategies and finite-size effects

The numerical optimization of tensors presented in the main text deals directly with systems of infinite size and then wraps them around a finite-size torus. Here we explore the alternative option of optimizing the tensors in the product state approximation to $|\Psi(n, L)\rangle$ directly on a torus, i.e., implementing the effect of periodic boundary conditions. We expect this optimization to be less efficient, therefore we can only access system sizes smaller than the

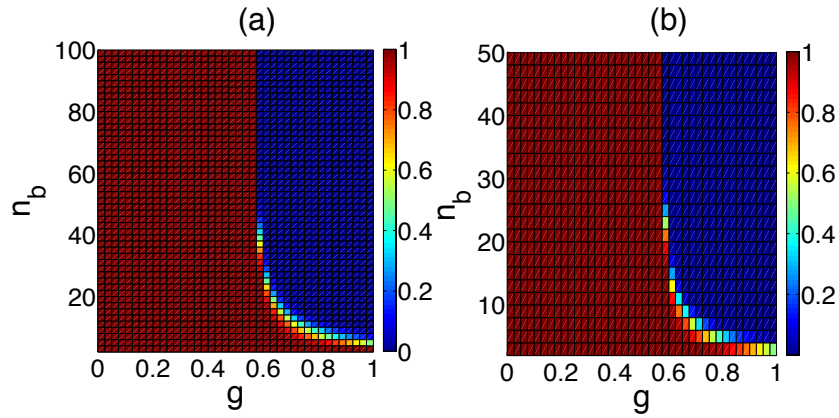


FIG. 9: (color online) $|E_\gamma|$ extrapolated from the scaling with L , as a function of the string tension g and the number of cylinders n_b , for toruses up to 100×100 sites, for the perturbed toric code on a square lattice and cylinders of width (a) $l = 1$, and (b) $l = 2$. Notice that both plots look almost identical, but the vertical axis in (b) spans half the values of the vertical axis in (a).

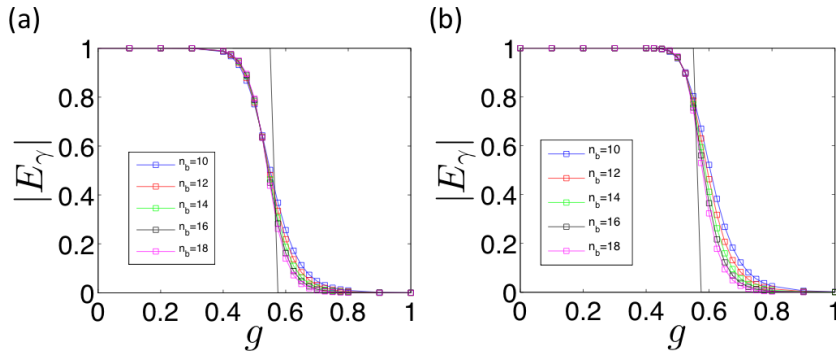


FIG. 10: (color online) E_γ estimated from the finite-size optimization, for the square lattice toric code state $|0, 0\rangle$, as a function of the string tension g and $n = 10 \dots, 18$. (a) $L = 20$, and (b) $L = 30$. Notice that there is a strong dependence on L , especially around the transition region. As expected, larger systems show a more robust topological phase, in turn tending towards the results in the main text for $L \gg 1$, which are represented by a black solid line.

ones mentioned in the main text. However, we also expect that finite-size corrections are more accurate, especially around the phase transition point. Thus, this is a valid and precise option to study finite-size corrections in E_G for small- and medium-size systems.

Operating first with an exact representation of the ground state and of product states on each cylinder of the torus we observe high accuracy of the MPS representation. This calculation, thus, validates our MPS approximation for the states within each cylinder. For toruses up to $L \approx 10$ and $n \gg 1$, we recover essentially the same results whenever the MPS bond dimension fulfills $\chi \approx 10 - 12$ (results not shown). Once this is clear, we have proceeded with the “finite-size” optimization over MPSs for larger toruses. As one can see in Fig.10, there is a strong dependence of E_γ on the system size in the transition region, as expected. The transition appears at larger g for increasing system size, while increasing the n_b makes this transition sharper. This can be used as an extra justification for the method used in the main text, which hits very efficiently the infinite-size limiting behavior even around the transition region. In a nutshell, by using systems of large size we rule out the possibility of any finite-size effect coming either from the optimization of the tensors or from the finite-size scaling on the torus.

In this work we have computed E_γ assuming a linear scaling with L for E_G and large L . Here we justify this approach by showing that non-linear corrections vanish in the large-size limit. We test directly the validity of the linear fit by computing its coefficient of determination R^2 . This is shown in Fig.11, for systems up to $L = 20$ and $n_b = 30$. The plot shows R^2 as a function of g and n_b , and one can see that a significant deviation from a

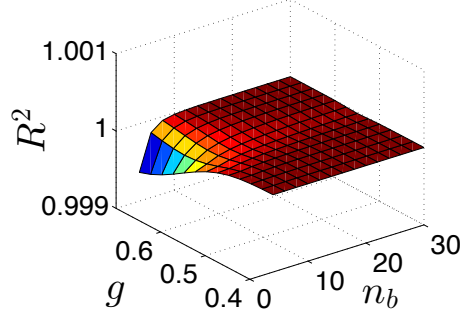


FIG. 11: (color online) R^2 for the linear fit. We observe that only at small system sizes the fit slightly deviates from almost-perfect linearity. The largest deviation is around the transition point, and vanishes for increasing system sizes.

perfect linear fit (for which $R^2 = 1$) happens only close to the transition point, and in fact vanishes as the system size increases.

Finally, in order to assess the validity of the linear fit we can also study deviations from it, e.g.,

$$E_G = E_0 - E_\gamma + \mathcal{O}(L^{-1}) + \mathcal{O}(L^{-2}), \quad (8)$$

which introduces non-linear terms in the fit. In Fig.12 we plot the coefficients for the $\mathcal{O}(L^{-1})$ and $\mathcal{O}(L^{-2})$ contributions to Eq.8. We see that the presence of these two terms is only significant for small systems around the transition point, vanishing for large system sizes. Notice also that the results shown in the main text were obtained for large systems, so that these non-linear contributions should be negligible. Such finite-size effects are only accessible in small- and medium-size systems, as shown here.

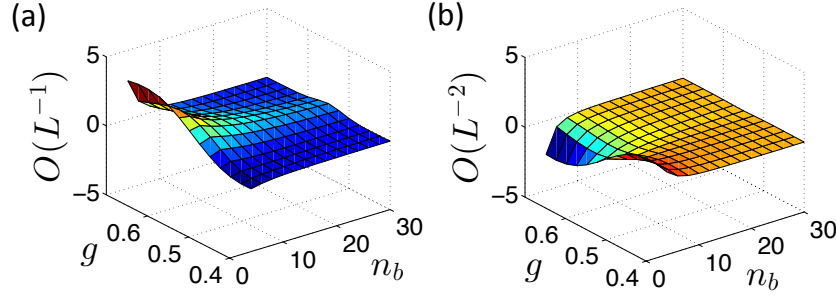


FIG. 12: (color online) (a) Contribution $\mathcal{O}(L^{-1})$ to the fit in Eq.8. Significant non-linear corrections appear only around the transition point, and vanish with for increasing sizes. (b) Contribution $\mathcal{O}(L^{-2})$ to the same fit. For $n_b \approx 10$, the correction is already negligible even around the transition point.

6. No continuous entanglement-loss in topological phases and local fidelity

In Ref.[6] it was argued that 1d many-body systems with conformally-invariant quantum critical points display continuous entanglement-loss along RG flows between fixed points. This was understood as a refinement of Zamolodchikov's famous c -theorem [7], recently generalized to 2d [8]. However, recent works have shown counter-examples to this behavior for different systems [9]. Here we provide similar results using the density of GE per block, which for large L corresponds to the linear term in our fits. To determine the nature of the RG flows in our systems, we

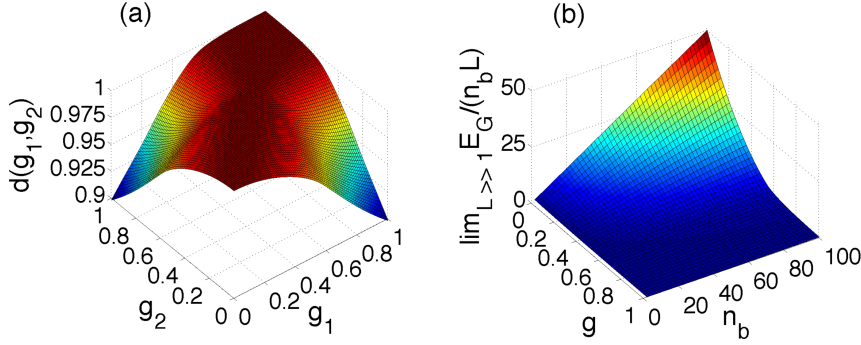


FIG. 13: (color online) perturbed toric code on the square lattice: (a) local fidelity diagram. Similar results are obtained for the honeycomb lattice. (b) Coefficient of L in the linear fit for large L , per block.

computed the local fidelity diagram in Fig. 13(a) [10]. The pinch-point in the local fidelity $d(g_1, g_2)$ [11] is in accordance with a continuous phase transition at $g^* \approx 0.56$, in turn corresponding to a critical and non-topological RG fixed point. Two more non-critical fixed points are present at $g = 0$, which is topological, and $g = \infty$, which is trivial. Coarse-graining drives the quantum state towards either $g = 0$ or $g = \infty$ depending on the phase, and thus $g = g^*$ is an unstable fixed point. As for the density of GE per block, in Fig. 13(b) we see that, in the topological phase, it increases as we move away from the phase transition point, so that the entanglement per site rises when flowing from $g = g^*$ towards $g = 0$. Albeit not a universal contribution, this already implies that there is no continuous reordering of quantum correlations at every infinitesimal RG step along the corresponding RG flow between these two fixed points, which rules out the possibility of continuous entanglement loss in the wave function.

7. Correlation length critical exponent ν from E_γ

Near criticality the only relevant length scale in the system is the correlation length, which scales as $\xi \sim |g - g^*|^{-\nu}$. For a finite-size system, the estimate g_c of the critical point g^* will depend on the system size L_s : $|g_c - g^*| \sim L_s^{-1/\nu}$. In our case, we have two different sizes n_b and L . If we take L very large, the remaining finite length-scale will be given by n_b , and thus in our case $|g_c - g^*| \sim n_b^{-1/\nu}$. We can test such an ansatz scaling to estimate the critical exponent ν from the behavior of $E_\gamma(n_b, L \rightarrow \infty)$, i.e., from the data in Fig. 4(a-c).

For instance, consider the perturbed toric code on the square lattice (Fig. 4(a)). For n_b between 12 and 60 we find that the best fit is $g_c = 0.55 + 3.83/n_b^{1.34}$ with $R^2 = 0.99992$, thus $\nu \sim 1/1.34$ (Fig. 14(a)). Between $n_b = 40$ and 60, the best fit gives $g_c = 0.55 + 5.58/n_b^{1.48}$ with $R^2 = 0.99999$, giving $\nu \sim 1/1.48$, close to $2/3$ (Fig. 14(b)). The critical exponent ν is thus estimated to fall roughly between 0.68 and 0.75. For comparison, other values found in topological transitions for the square-lattice toric code model are the Ising value $\nu \sim 0.63$ for a parallel magnetic field, and also any value between $\nu \sim 0.63$ and $\nu \sim 1$ along a multicritical line for an arbitrary field [12]. In our case, we believe that errors come from the finite number of grid points for g and the procedure of estimating g_c (which we determine as the value of g at $|E_\gamma| \sim 0.5$ by interpolating the available data). The accuracy can be improved by computing more data, but in any case, the analysis suggests that the transition is continuous, in accordance with our fidelity results in Fig. (13).

8. Tensor network methods to compute Rényi entropies on infinite cylinders

The Rényi entropy between a subsystem with reduced density matrix ρ and the rest of the system is given by

$$S^{(n)} = \frac{1}{1-n} \log(\text{tr}(\rho^n)), \quad (9)$$

with n the Rényi entropy index. The limit $n \rightarrow 1$ coincides with the usual von Neumann (or entanglement) entropy $S^{(1)} = -\text{tr} \rho \log \rho$, whereas the limit $n \rightarrow \infty$ corresponds to the so-called infinity Rényi entropy, or single-copy entanglement, $S^{(\infty)} = -\log \nu_1$, with ν_1 the largest eigenvalue of ρ . In Ref. [13] it was proven that all these entropies have the same topological contribution, so that any of them can be used to identify the topological nature of a given state.

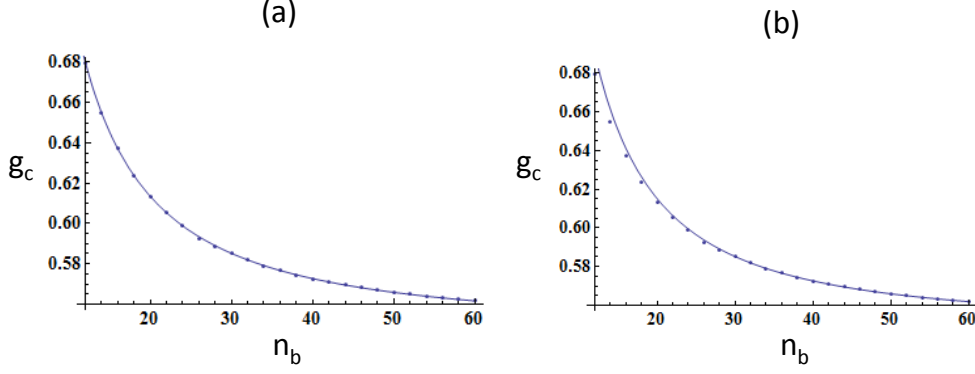


FIG. 14: (color online) (a) correlation length fit for n_b between 12 and 60; (b) correlation length fit for n_b between 40 and 60 (whole range of n_b displayed).

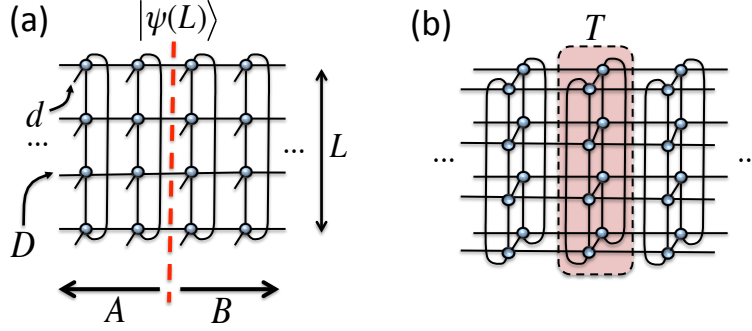


FIG. 15: (color online) (a) 2d PEPS on an infinite cylinder of circumference L . (b) Transfer matrix T .

Because of this, in combination with their apparent simplicity, Rényi entropies have become quite common tools to evaluate the presence of topological order in quantum many-body systems. For instance, the 2-Rényi entropy is a usual approach in Quantum Monte Carlo [14], whereas in tensor networks, and especially in 2d PEPS, both the 2-Rényi entropy and the infinite Rényi entropy (or single-copy entanglement) are easily accessible quantities. This follows, e.g., from the approach explained in Ref.[15], which relies on wrapping the 2d PEPS around a cylinder of circumference L , and considering a non-contractible bipartition of the cylinder in two halves.

Let us be more precise with the tensor network calculation: we start with a 2d PEPS $|\psi(L)\rangle$ on a cylinder of circumference L . For simplicity, we assume that the cylinder is infinitely long, though finite systems can also be considered easily. We partition the cylinder into two half-infinite pieces A and B , see Fig.15(a). As explained in Ref.[15], the reduced density matrix of half an infinite cylinder (e.g. A) is given by

$$\rho = U \sqrt{\sigma_A^T \sigma_B} \sqrt{\sigma_A^T} U^\dagger, \quad (10)$$

with $\sigma_{A/B}$ the reduced density operators in A/B for the virtual spaces across the bipartition, and U an isometry. When the appropriate symmetries are present, as in the cases analyzed here, one has $\sigma_A = \sigma_B \equiv \sigma$, and therefore

$$\rho = U \sigma^2 U^\dagger. \quad (11)$$

Notice that this readily implies that ρ and σ^2 are isospectral, since the isometries do not change non-zero eigenvalues, and therefore the Rényi entropies only depend on the eigenvalues of σ . And what is more: in terms of σ the Rényi entropies now read

$$S^{(n)} = \frac{1}{1-n} \log(\text{tr}(\sigma^{2n})). \quad (12)$$

Thus, computing $S^{(n)}$ amounts to calculating σ , its powers, and its trace [17].

The calculation of σ on an infinite cylinder for a 2d PEPS is a well-posed tensor network problem, since σ is nothing but the dominant (left or right) eigenvector of the PEPS transfer matrix T , see Fig.15(b). This can be solved using

many different strategies. Here we choose a similar approach to the one described in the main text for the GE: we compute this dominant eigenvector using the iTEBD method for non-unitary evolutions [1, 2]. The resulting dominant eigenvector can be written as an MPO of bond dimension χ , which is then wrapped around a circle of length L , and constitutes our approximated σ . The computational cost of this calculation is $O(\chi^3 D^6 + \chi^2 D^8)$ [16].

Next, by combining the obtained MPO for σ with Eq.12 it is easy to see that, again, the calculation of any Rényi entropy $S^{(n)}$ can be reduced to some standard tensor network problem, see Figs.16 and 17. From here, the calculation strategy differs depending on whether we are interested in finite- n , or in the limit $n \rightarrow \infty$. The details of both cases are as follows:

Finite- n Rényi entropies

In this case the calculation amounts to computing the tensor network contraction from Fig.16, taking into account the normalization of σ^2 . Formally, the numerator inside the logarithm amounts to the contraction of a 2d tensor network on a torus of size $n \times L$, thus being quite similar to some of the contractions that were involved in the calculation of the GE in the main text. Therefore, we simply use now the same approach that was used there, i.e., we approximate the repeated multiplication of MPOs using iTEBD as explained in the first section of this supplementary material. After exactly $2n$ iterations we stop, and wrap the resulting MPO with bond dimension χ' around a circle of size L . The total computation time for this approach scales as $O(2n(\chi^2 \chi'^2 D^3 + \chi^3 \chi'^3 D^2) + L\chi'^3)$.

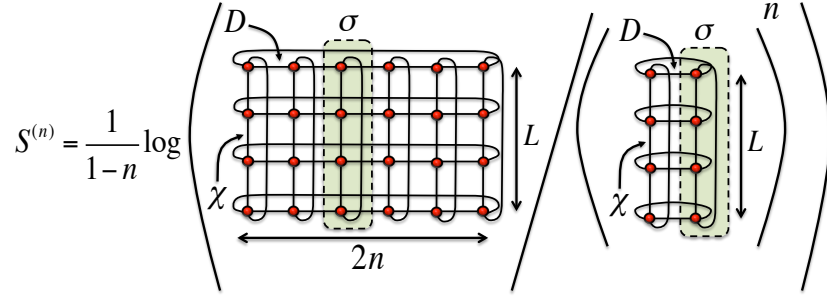


FIG. 16: (color online) tensor network diagrams corresponding to the finite- n Rényi entropy.

∞ -Rényi entropy (single-copy entanglement)

The case $n = \infty$ deserves special attention. In principle, it should be possible to use the same trick as for finite- n above, taking the limit of a very large n until some convergence is reached. However, even if correct, such an approach is not necessarily the most efficient one. To understand this, simply notice that the largest eigenvalue ν_1 of ρ also corresponds to the largest (normalized) eigenvalue of σ^2 , i.e.,

$$\nu_1 = \frac{v_L^T \sigma^2 v_R}{v_L^T v_R}, \quad (13)$$

with v_L and v_R respectively the left and right dominant eigenvectors of σ . Since σ is given in the form of an MPO with periodic boundary conditions, it turns out that finding such dominant eigenvectors is also a standard 2d tensor network problem which we solve as done many times before: using iTEBD and wrapping the resulting MPS for v_L and v_R , with bond dimension χ' , around a circle of size L . In the end, $S^{(\infty)}$ is computed as in the diagram in Fig.17. The overall computational cost of this approach is $O(\chi^3 \chi'^3 D^3 + L\chi^5 \chi'^5 D)$.

Remarks

Some remarks are in order. First, if we are interested in extracting the topological component, we just proceed by doing finite-size scaling with L , fitting the results to a linear function, and extrapolating the result down to $L \rightarrow 0$, exactly as we did for the GE. Second, the calculations of Rényi entropies with 2d PEPS can of course be improved in

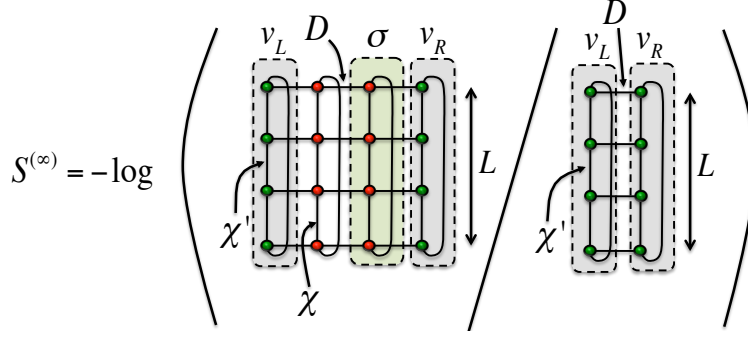


FIG. 17: (color online) tensor network diagrams corresponding to the $n = \infty$ Rényi entropy.

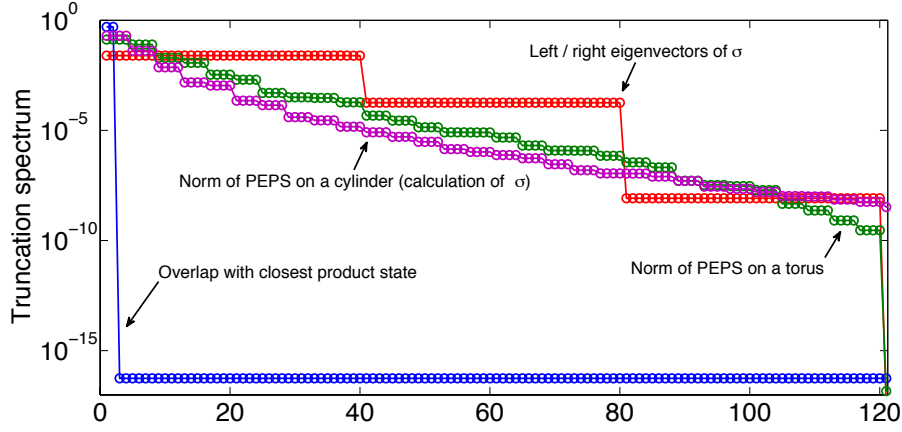


FIG. 18: (color online) Different spectra to be truncated in the evaluation of E_G or the Rényi entropies, for the perturbed toric code on a square lattice with $g = 0.55$.

accuracy, especially if the correlation length is large (e.g. close to criticality). However, the practical drop in efficiency is very significant. And what is more: the same improvements that can be applied to Rényi entropy calculations can also be used, if necessary, to improve the accuracy in computing the GE. Third, we have observed that the calculations of the n -th Rényi entropies are extremely sensitive to truncations in the associated bond dimensions, which becomes especially important when n gets ‘large’. In practice, this means that we have been unable to produce sensible results for the topological contribution of Rényi entropies for $n > 3$ (except for infinity) because we cannot reach sufficiently large bond dimensions with our computing resources. This is to be contrasted with the remarkable robustness and accuracy of the GE, already for small bond dimensions. In other words: for a comparable value of bond dimensions and computation time, the topological GE outperforms in accuracy the topological Rényi entropies by far, especially close to a quantum critical point.

9. Truncation errors in E_G and Rényi entropies.

As explained in the main text, our method to compute E_G uses mainly single-layer contractions of a $2d$ tensor network. Such contractions appear in the calculation of the overlap between the optimal product state and the $2d$ PEPS, and can be computed very efficiently and as well as very accurately. Moreover, they are also numerically more stable than the usual double-layer contractions needed to compute, e.g., the norm of the $2d$ PEPS. Almost half of the numerical manipulations to evaluate E_G rely on such single-layer contractions. Moreover, the necessary double-layer contractions to evaluate E_G are only those to compute the norm of a PEPS, which is a single scalar quantity (unlike an operator that is re-used). All in all, this makes the evaluation of E_G inherently very accurate and robust. A different scenario is present for Rényi entropies, where the only fundamental object σ is computed from a double-layer contraction. Such object σ is further used in more calculations, which in practice means that there is a concatenation of errors if σ itself is not computed extremely accurately. In practice, this means that Rényi entropies can be prone to

a larger error than the E_G whenever we have quantum states with a lot of entanglement, especially near a quantum phase transition, and this is indeed what we see in the main text.

To further justify this picture, we have plotted in Fig.18 the first 120 values of the spectrum to be truncated in different steps of the calculations mentioned above. In the figure one can see that, while the spectrum for the single-layer contraction decays extremely fast, all the rest decay very slowly. As claimed, this means that truncation effects are less dramatic for E_G , which depends partly on truncations of single-layer calculations spectra and do not re-use objects computed from double-layer calculations. Since such single-layer spectra decay very fast, they can also be truncated accurately with a small truncation parameter, and hence the overall calculation is not only more accurate, but also faster than the one of any of the Rényi entropies, as claimed.

-
- [1] G. Vidal, Phys. Rev. Lett. **98**, 070201 (2007).
 - [2] R. Orús, G. Vidal, Phys. Rev. B **78**, 155117 (2008).
 - [3] A. Y. Kitaev, Annals of Physics 303, 2-30 (2003).
 - [4] R. Orús, Annals of Physics **349**, 117158 (2014).
 - [5] R. Orús *et al.*, New J. Phys. **16** 013015 (2014).
 - [6] J.I. Latorre *et al.*, Phys. Rev. A **71** 034301 (2005); R. Orús, Phys. Rev. A **71**, 052327 (2005), erratum-ibid **73**, 019904 (2006).
 - [7] A. B. Zamolodchikov, JETP Lett. **43** 730 (1986);
 - [8] I. R. Klebanov, S. S. Pufu, B. R. Safdi, arXiv:1105.4598.
 - [9] B. Swingle, arXiv:1307.8117; S. Santra *et al.*, arXiv:1310.6490.
 - [10] P. Zanardi and N. Paunković, Phys. Rev. E **74**, 031123 (2006); H.-Q. Zhou, J.P. Barjaktarevic, cond-mat/0701608; H.-Q. Zhou, J.-H. Zhao, B. Li, arXiv:0704.2940; H.-Q. Zhou, arXiv:0704.2945; H.-Q. Zhou, R. Orús, G. Vidal, Phys. Rev. Lett. **100**, 080601 (2008).
 - [11] If $|\Psi(g)\rangle$ is the PEPS with parameter g on a 2d lattice of N sites, then $|\langle\Psi(g_1)|\Psi(g_2)\rangle| \sim d(g_1, g_2)^N$ for $N \gg 1$.
 - [12] S. Dusuel *et al.*, Phys. Rev. Lett. **106**, 107203 (2011).
 - [13] S. T. Flammia *et al.*, Phys. Rev. Lett. **103**, 261601 (2009).
 - [14] S. V. Isakov *et al.*, Nature Physics **7**, 772 (2011); X. Chen *et al.*, Phys. Rev. B **82**, 165119 (2010); S. Morampudi, C. von Keyserlingk, F. Pollmann, arXiv:1403.0768; J.-M. Stéphan, G. Misguich, V. Pasquier, J. Stat. Mech. P02003 (2012).
 - [15] J. I. Cirac *et al.*, Phys. Rev. B **83**, 245134 (2011).
 - [16] J. Jordan *et al.*, Phys. Rev. Lett. **101**, 250602 (2008); R. Orús, G. Vidal, Phys. Rev. B **80**, 094403 (2009); S. Dusuel *et al.*, Phys. Rev. Lett. **106**, 107203 (2011); M. D. Schulz *et al.*, New J. Phys. **14**, 025005 (2012).
 - [17] In fact, with this approach one could also compute $S^{(1/2)}, S^{(3/2)}, \dots$